# Miniaturization of InGaP/InGaAs/Ge solar cells for microconcentrator photovoltaics

Pierre Albert, Abdelatif Jaouad, Gwenaëlle Hamon, Maïté Volatier, Christopher E Valdivia, Yannick Deshayes, Karin Hinzer, Laurent Béchou, Vincent Aimez, Maxime Darnon

Revised: 24 December 2020 | Accepted: 30 March 2021

DOI: 10.1002/pip.3421

RESEARCH ARTICLE

PROGRESS IN PHOTOVOLTAICS WILEY

# Miniaturization of InGaP/InGaAs/Ge solar cells for micro-concentrator photovoltaics

Pierre Albert[1,2,3] | Abdelatif Jaouad[1,2] | Gwenaëlle Hamon[1,2] | Maïté Volatier[1,2] | Christopher E. Valdivia[4] | Yannick Deshayes[3] | Karin Hinzer[4] | Laurent Béchou[1,2,3] | Vincent Aimez[1,2] | Maxime Darnon[1,2]

[1]Laboratoire Nanotechnologies Nanosystèmes (LN2)–CNRS, Université de Sherbrooke, 3000, boulevard de l'Université, Sherbrooke, Québec, J1K 0A5, Canada

[2]Institut Interdisciplinaire d'Innovation Technologique (3IT), Université de Sherbrooke, 3000, boulevard de l'Université, Sherbrooke, Québec, J1K 0A5, Canada

[3]Laboratoire de l'Intégration du Matériau au Système (IMS)–CNRS UMR 5218, Université de Bordeaux, Talence, France

[4]SUNLAB Centre for Research in Photonics, University of Ottawa, Ottawa, Ontario, Canada

**Correspondence**
Maxime Darnon, Laboratoire Nanotechnologies Nanosystèmes (LN2)–CNRS, Université de Sherbrooke, 3000, boulevard de l'Université, Sherbrooke, J1K OA5, Québec, Canada.
Email: maxime.darnon@usherbrooke.ca

**Funding information**
Natural Sciences and Engineering Research Council of Canada, Grant/Award Number: 497981; Université Grenoble Alpes; INSA Lyon; Université de Sherbrooke

## Abstract

Micro-concentrator photovoltaic (CPV), incorporating micro-scale solar cells within concentrator photovoltaic modules, promises an inexpensive and highly efficient technology that can mitigate the drawbacks that impede standard CPV, such as resistive power losses. In this paper, we fabricate micro-scale multijunction solar cells designed for micro-CPV applications. A generic process flow, including plasma etching steps, was developed for the fabrication of complete InGaP/InGaAs/Ge microcells with rectangular, circular, and hexagonal active areas down to 0.089 $mm^2$ (0.068-$mm^2$ mesa). Large cells (>1 $mm^2$) demonstrate good electrical performance under one sun AM1.5D illumination, but a degradation in the open-circuit voltage ($V_{OC}$) is observed on the smallest cells. This effect is attributed to perimeter recombination for which a passivation effect by the antireflective coating partially recovers the $V_{OC}$. The $V_{OC}$ penalty for small cells is also reduced under high-intensity illumination, from 3.8% under sun to 1.0% at 974 suns. High intensity illumination yields an efficiency of 33.8% under 584 suns for a 0.25-$mm^2$ and microcells are expected to show higher efficiency than standard cells under very high concentration.

**KEYWORDS**
device characterization, III-V semiconductors, microcells, micro-CPV, microfabrication, multijunction solar cells, perimeter recombination, triple-junction solar cells

## 1 | INTRODUCTION

Concentrator photovoltaic (CPV) systems are based on the use of high efficiency multijunction solar cells (MJSC) and optical collectors that typically concentrate the sunlight 300–1000 times to boost cell efficiency and to reduce semiconductor area (typically 1 $cm^2$ down to a few $mm^2$). Although champion solar cells have reached efficiencies of 44.4% and 46.0% for three- and four-junction cells,[1] respectively, CPV has not reached the targeted levelized cost of electricity (LCOE) of conventional silicon flat-panel photovoltaic (PV) modules. Indeed, CPV LCOE was evaluated between 94 $/MWh and 177 $/MWh in 2017 whereas an average PV LCOE of 51 $/MWh was reached in 2019.[2,3]

In recent years, micro-scale concentrator photovoltaics (micro-CPV) based on <1 $mm^2$ cells has emerged as an approach that could offer an advantageous cost.[4] First, micro-CPV modules are lighter and more compact than standard-CPV modules, facilitating logistics and installation, and therefore leading to a reduced carbon

footprint and balance of system cost.[5] The miniaturization of CPV cells and modules also offers the opportunity to use simplified assembly processes that can be borrowed from LED manufacturing for example, as heat distribution on the carriers is more homogeneous with smaller cells.[6] The module miniaturization also benefits to optical elements: an increase of more than 5% in absolute optical efficiency is expected for low-cost optics when reducing cell size from 1 mm to 100 μm on a side.[7] Finally, reducing the cell surface decreases the total current, mitigating resistive losses that scale with the square of the current.[8,9] A fair indicator of the module integration success is the module-to-cell efficiency ratio (MTC), calculated as the module efficiency divided by the cell efficiency. While MTC of commercial standard CPV modules is typically between 65% and 75%, miniaturized modules have shown MTC in the range 71%–87%.[10] Consequently, micro-CPV modules have already demonstrated high efficiency (>35%) with a record of 41.7%.[11–18] A summary of existing high-performance micro-CPV modules is reported in Table 1.

Although micro-CPV and microcells appear to be good candidates for the next generation CPV, some challenges remain. Indeed, high-performance fabrication techniques must be adapted to allow small size together with low cost. Surface recombination along the side-wall perimeter is known to have a greater performance impact on solar cells with a high perimeter-to-area ratio (i.e., very small cells), mostly due to a high density of surface states (i.e., $>10^{13}$ $cm^{-2}$).[19] The role of perimeter recombination in cells, which particularly affects their voltage, was studied in single junction,[20–22] in the subcells that compose a three-junction cell,[23] and in three-junction structures.[11,12,24] An effective reduction of GaAs surface states density can be obtained by sulfur passivation, plasma treatments, or atomic layer deposition (ALD).[25] In addition, Ref.[24] showed that front contact pads used for typical wirebonding assembly utilize a considerable fraction of the microcells area. Metal contacts that shade 39% of the cell cause a reduction in voltage equivalent to the effect of perimeter recombination in microcells with a 0.11-$mm^2$ mesa area. However, such a high shading seems impractical in real systems and therefore perimeter recombination is the main loss to address in microcells. Due to these challenges, no fully fabricated (i.e., singulated) three-junction solar cell with a total area of less than 0.3 $mm^2$ has been reported in the literature, to the author's knowledge.

In this paper, we report on the fabrication and the characterization of high-efficiency three-junction solar cells with <1-$mm^2$ area. A specific fabrication process based on microelectronic techniques was developed to allow the fabrication of microcells with various geometries (rectangular, circular, and hexagonal) and with area down to 0.068 $mm^2$. We discuss the relevance of the developed process and the impact of cell dimensions as well as the passivation effect of the antireflective coating on electrical performance. Characterization is done under one sun and high-intensity light. It is shown that performance degrades with cell size reduction and is attributed to perimeter recombination. A performance recovery is demonstrated when cells are coated with an antireflective coating and operating under concentrated light. Flash measurements show good performance of the fabricated microcells and the origin of the efficiency limitation under very high concentration is not attributed to resistive losses.

## 2 | CELL FABRICATION

### 2.1 | Process flow

A process flow that was developed to fabricate microcells is illustrated in Figure 1. We used commercial Ge wafers of three-junction lattice-matched InGaP/InGaAs/Ge to develop the process in this study as they are a standard baseline design in CPV (see Figure 1A). However, all processes can be generalized to other materials used in multi-junction cell structures. The first step is the evaporation of Pd/Ge/Ti/Pd/Al (50/100/50/50/500 nm) metal stack, as developed in Huo and Rey-Stolle,[26] to form the front electrode. A lift-off process defines the shape, grid pitch, and dimensions of these contacts, as shown in Figure 1B and presented in Albert et al.[27] Then, a Ti/Al (50/200 nm) metallization is deposited on the backside of the wafer, resulting in the base contact as illustrated in Figure 1C. Cells are then electrically

**TABLE 1** State-of-the-art for micro-CPV modules with associated efficiency, lens area and/or concentration, cell mesa area, and structure

| Groups (year) | Module efficiency | Lens area ($cm^2$) /concentration (suns) | Mesa area | Cell structure | Ref. |
|---|---|---|---|---|---|
| Panasonic, Solar Junction (2014) | 34.7% | 1 × 1/N.C | 600 × 600 $\mu m^2$ | 3 J cell: InGaP/GaAs/GaInNAsSb | 11 |
| Solar Junction, Panasonic (2014) | 34.7% | 1 × 1/N.C. | 550 × 550 $\mu m^2$ | 3 J cell: InGaP/GaAs/GaInNAsSb | 12 |
| University of Illinois at Urbana-Champaign, Semprius, Solar Junction (2014) | 36.5% | 2 × 2/1000 | 600 × 600 $\mu m^2$ | 4-terminals, 4 J-stacked cell: InGaP/GaAs/GaInNAsSb on Ge | 13 |
| Semprius Commercial (2016) | 34.9% | N.C/1111 | 600 × 600 $\mu m^2$ | 3 J cell: GaAs-based | 14 |
| Panasonic (2015) | 35.9% | 1 × 1/150 | 970 × 970 $\mu m^2$ | 3 J cell: InGaP/GaAs/GaInNAsSb | 15 |
| CEA-Liten (2017) | 33.4% | 19 × 19/1000 | 600 × 600 $\mu m^2$ | 3 J cell: InGaP/(In)GaAs/Ge | 16 |
| EPFL (2017) | 36.4% | 0.687/N.C. | 600 × 600 $\mu m^2$ | 3 J cell: InGaP/GaAs/GaInNAsSb | 17 |
| NRL (2017) | 41.2% | 3.142/744 | 755 × 805 $\mu m^2$ | 4-terminals, 5 J-stacked cell: InGaP/GaAs/InGaAsNSb on GaSb/InGaAsSb | 18 |

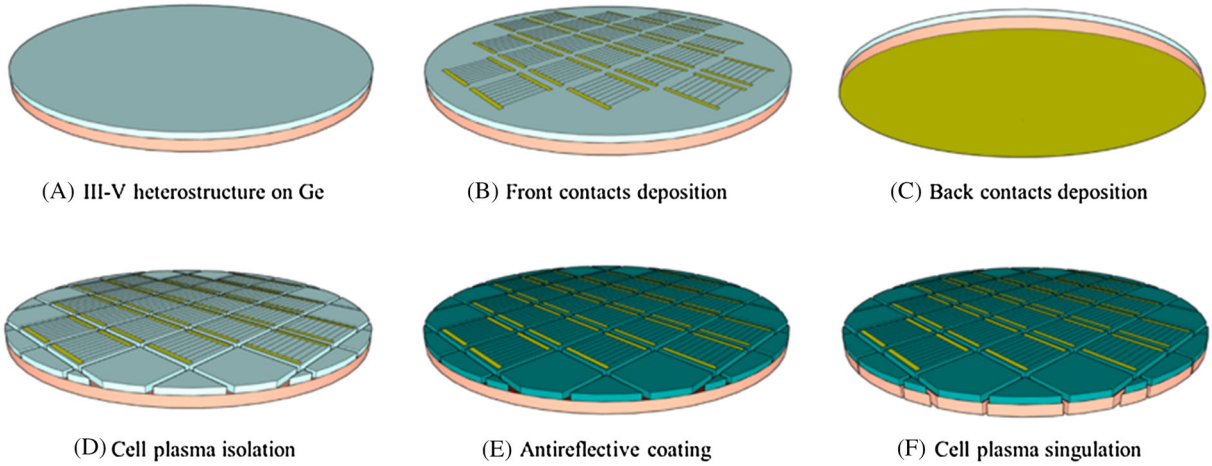


**FIGURE 1** Main steps in the microcell fabrication process flow [Colour figure can be viewed at wileyonlinelibrary.com]

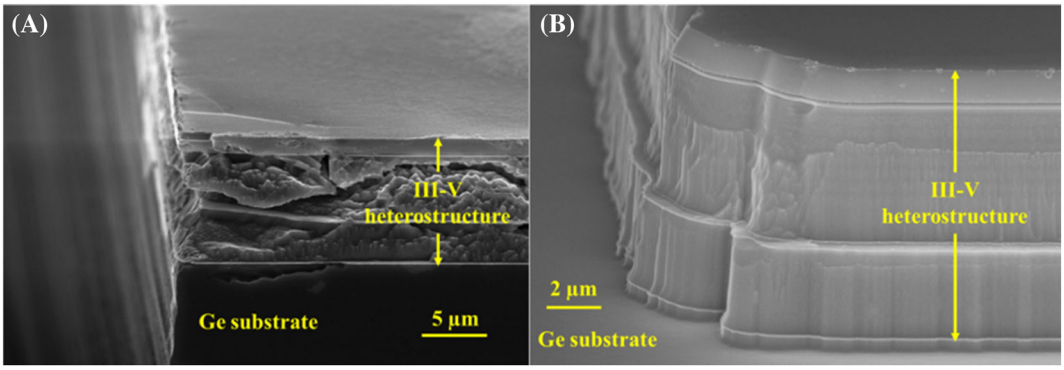


**FIGURE 2** Scanning electron microscope (SEM) tilted views of cell sidewalls (mesas) isolated by (A) saw dicing (precut + chemical cleaning) and (B) plasma etch (precut + chemical cleaning) [Colour figure can be viewed at wileyonlinelibrary.com]

isolated by forming mesas on the front face by plasma etching as shown in Figure 1D and detailed in Section 2.2. A $SiN_xH_y/SiO_xH_y$ bi-layer is deposited then by plasma enhanced chemical vapor deposition (PECVD) to passivate the surface and to ensure an effective anti-reflective coating (ARC), thereby increasing electrical performance[28] (Figure 1E). The ARC is then opened by plasma etching on the busbars to access the electrical pads. The plasma singulation ends the micro-cell fabrication as seen in Figure 1F and detailed in Section 2.3.

## 2.2 | Cell isolation

In a standard process, cells are mechanically isolated and singulated in a single step (fullcut only) or two steps (precut + fullcut) if a passivation/antireflective coating is required on the cell sidewalls. Saw dicing remains the mainstream method to isolate and separate CPV cells, although laser (fullcut only), combination of wet etching (pre-cut) and laser (full cut), or plasma technology can also be used to implement this step. However, for microcell fabrication, saw dicing is not applicable due to the reasons below.

First, the fragililty of the III-V/Ge cell structure is susceptible to defect generation as a result of saw dicing. Chipping defects left by the saw at the mesa sidewalls, as illustrated in Figure 2A (isolation precut only), create recombination centers that can lead to electrical performance degradation and reliability issues. Saw precut for cell isolation is consequently not recommended and manufacturers suggest the device-free zone to be ~2.5–3 times larger than the blade width.[29] Presently, dicing saw can be as narrow as 15 µm but are typically 50–120 µm wide.[30]

Second, the wafer yield decreases dramatically as cell size decreases, as illustrated in Figure 3. With these parameters, saw dicing of 0.068 $mm^2$ cells (the smallest area reported in this paper) would produce a wafer yield of only 52.1%, which is unacceptable for such expensive semiconductors. However, a yield of 65.9% and 89.4% are achievable for laser dicing and plasma dicing, respectively.

Third, the probability of tearing chips off the wafer is increased for small devices. Cooling water pressure together with mechanical forces and vibrations generated by the saw rotation are harsh and make the saw dicing difficult for very small chips. Whereas higher-adhesion die attach tape can be envisaged, the further die picking is

complicated due to the fragile materials involved in multijunction structure.[31] In addition, saw dicing generates linear channels that force the fabricated cells to be rectangular, which may be inadequate depending on the incoming light profile. Finally, large numbers of particles are not extracted by the water flow and can attach to the surface of the diced chip.

Accordingly, isolation of microcells requires a soft advanced microfabrication technique such as plasma etching, as developed in the recent years in our group.[32–36] In this work, a $Cl_2/SiCl_4/H_2$-based inductively coupled plasma etch was chosen for isolating the whole heterostructure of Figure 1D. Indeed, the hydrogen present in the plasma is known to partially passivate the etched surfaces, which results in lower electrical losses in solar cells.[34] The contact layer, a highly doped InGaAs film, is then chemically etched in a $NH_4OH:H_2O_2:H_2O$ (9:9:240) solution for 45 s. Figure 2B shows a plasma-etched cell mesa sidewall. First, the high anisotropy of the developed process can be observed, generating a high verticality of the mesa sidewalls, which is particularly important to ensure current matching between the subcells of such small devices. This anisotropy is possible since the process is highly ion-driven and the selectivity of the used plasma chemistry to the various materials that compose the heterostructure (~10 μm) is very low. This parallel and fast process (average etch rate >1 μm/min) also offers the possibility to achieve photolithography-defined patterns and thus does not limit cells shapes to rectangles. Such anisotropic isolation and versatile devices shape is not possible with wet etching, due to the preferential etching along crystalline directions of the different III-V materials.[37] In addition, Figure 2B shows that the mesa sidewalls exhibit a smoother surface than with saw dicing, suggesting the surface state density is lower and therefore less surface recombination at the perimeter of the cells is expected.

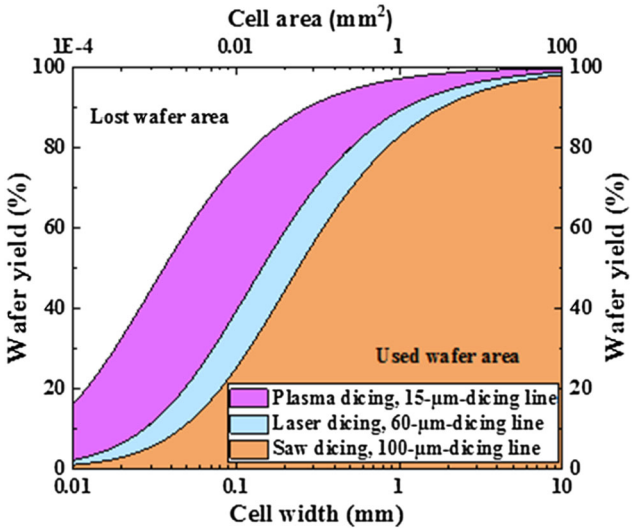


**FIGURE 3** Wafer yield as a function of cell dimensions for different dicing techniques. Plasma dicing lines are 15 μm (10-μm cut + 2 × 2.5-μm-defect-free zone), laser dicing lines are 60 μm (40-μm cut + 2 × 10-μm recast-and-defect-free zone), and saw dicing lines are 100 μm (40-μm cut × 2.5 defect-free-zone factor)[29,30,38] [Colour figure can be viewed at wileyonlinelibrary.com]

## 2.3 | Cell Singulation

The cell fabrication process ends with singulation to separate the completed cells. Alternatives to diamond sawing are desirable for the same reasons as the isolation cut. Laser ablation technology offers the ability to dice non-rectangular small chips with a relatively lower defect generation and thinner cut lines. However, a contamination of the diced wafer remains and heat generation during ablation can cause defects.[38] Wet etching for singulating cells was not considered given the low etch rates of germanium (<1 μm/min).[39] Moreover, such isotropic etching would induce trenches width of at least 170 μm, which is hardly conceivable for microcells fabrication. Whereas laser dicing provides a higher wafer yield than saw dicing, it is lower than for plasma-diced small cells, as seen in Figure 3. Consequently, in this work, we also proposed plasma etching for the singulation step (full cut). The process involves a time multiplexed

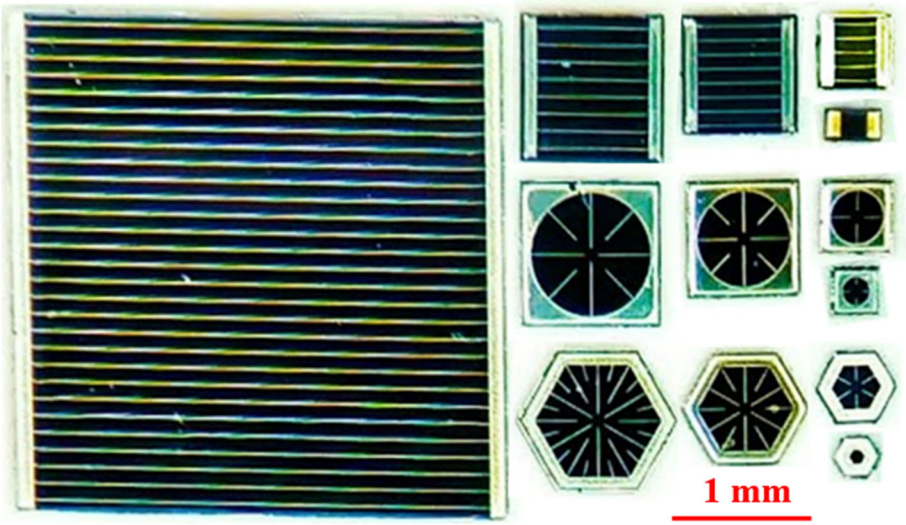


**FIGURE 4** Optical image of fabricated microcells. The largest cell (square) is 12.53 $mm^2$ (12.25-$mm^2$ mesa) and the smallest one (hexagonal) is 0.089 $mm^2$ (0.068 $mm^2$-mesa) [Colour figure can be viewed at wileyonlinelibrary.com]

(Bosch) plasma process with alternative steps of etching with $SF_6/O_2$ and passivation with $C_4F_8$ to cut through the Ge wafer. This allows deep etching with a relatively high etch rate (>3 μm/min) of high aspect ratio (*AR*) trenches (up to 17).[32] Whereas in this work trenches of 50 μm-width were successfully etched through the 170-μm-thick Ge substrate, trenches as small as 10 μm can be etched without generating defects.[32] After this final manufacturing step, devices are typically 20 μm wider than the cell mesa due to 10 μm photolithography margins.

After the cells are singulated, they can be electrically characterized before being assembled in modules. Figure 4 shows a top view of completed triple-junction solar cells where the largest mesa is 3.5 mm on a side (square cell, 12.53-$mm^2$ total area, front contact shading = 10.3%) while the smallest mesa is 160 μm on a side (hexagonal cell, 0.089-$mm^2$ total area, front contact shading = 72.9%). Electro-optical characterization of micro-CPV cells is not straightforward. Besides setups (microscopes/cameras and probing for example) that need to be adapted, solar simulators and flash testers must demonstrate a highly homogeneous light and even AAA class facilities are unlikely to meet requirements without additional effort. Indeed, a high light-uniformity is required when considering microcells due to their reduced surface to average the incoming light. A usual calibration of solar simulators and flash testers, to ensure current-matching between subcells, use isotype cells which dimensions are not compatible with microcells for which local intensity and spectrum may vary. Moreover, some measurements, such as quantum efficiency (QE), which systems typically use >1-mm spots, require further development to be applicable to microcells.

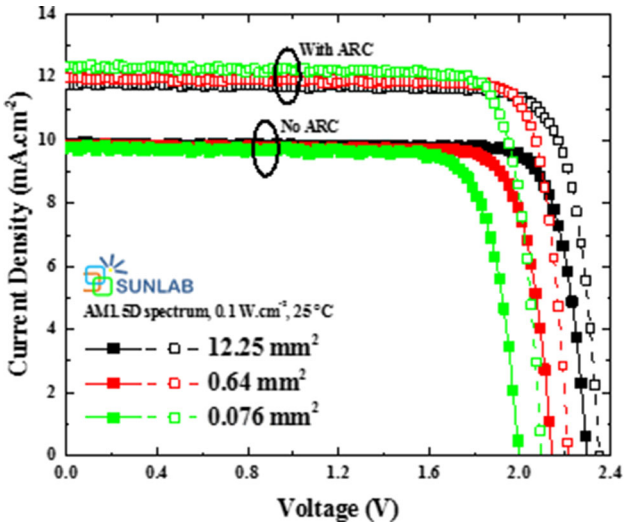


**FIGURE 5** One-sun current density vs voltage characteristics of rectangular cells depending on their mesa area (12.25, 0.64, and 0.076 $mm^2$) and the presence of an ARC [Colour figure can be viewed at wileyonlinelibrary.com]

## 3 | CELL CHARACTERIZATION

### 3.1 | One sun measurements

The cells fabricated with the process described in Section 2 were characterized under one sun at 25°C with AM1.5D (ASTM G173) spectrum with an Oriel SOL3A-CPV class AAA solar simulator. Figure 5 depicts the current density (*J*) vs voltage (*V*) characteristics of rectangular cells with different sizes, and with and without a passivating ARC (one sample per size). The surface considered for current density calculation is the active area, defined as the mesa area excluding busbars area. First, a standard-size cell (12.25-$mm^2$ mesa area) with ARC shows good electrical performance under one sun (open-circuit voltage $V_{OC}$ = 2.350 V; fill factor *FF* = 82.7%, short-circuit current density $J_{SC}$ = 12.40 mA $cm^{-2}$) validating the fabrication process. Without ARC, the 12.25 $mm^2$ cell generates 19.1% less current due to higher reflection and the slight variations of $J_{SC}$ between cells are due to illumination non-uniformity, which particularly affects small cells. The $V_{OC}$ is also 53 mV lower than with ARC, which is attributed to the lower short circuits current and to higher surface recombination on the non-passivated surfaces. When the dimensions of the solar cell decreases from 12.25 $mm^2$ down to 0.076 $mm^2$, the $V_{OC}$ of the cells decreases from 2.35 V down to 2.096 V (−10.79%) for the cell with ARC and from 2.297 V down to 1.995 V (−13.16%) for the cell without ARC (see Tables 2 and 3). We can notice that such a decrease is more pronounced on the cells without ARC, confirming that the ARC partly passivates the surface of the cell sidewalls.

Figure 6 shows that the trend of $V_{OC}$ of single rectangular solar cells both with and without ARC, plotted against the perimeter-to-area ratio (defined as $P_{mesa}/A_{mesa}$, where $P_{mesa}$ and $A_{mesa}$ are the mesa perimeter and area, respectively) in a semi-logarithmic scale, has a quasi-linear decrease. The same trend was observed for cells with other geometries (see Appendix A).

**TABLE 2** Electrical parameters of fabricated rectangular cells with and without ARC

| Electrical parameter (AM1.5D, 0.1 W·$cm^{-2}$, 25°C) | Presence of ARC | Mesa area 12.25 $mm^2$ | 0.64 $mm^2$ | 0.076 $mm^2$ |
|---|---|---|---|---|
| $V_{OC}$ [V] | NO ARC | 2.297 | 2.142 | 1.995 |
| | WITH ARC | 2.350 | 2.213 | 2.096 |
| $J_{SC}$ [mA.$cm^{-2}$] | NO ARC | 9.90 | 9.84 | 9.77 |
| | WITH ARC | 11.79 | 12.01 | 12.36 |
| *FF* [%] | NO ARC | 84.05 | 82.61 | 81.11 |
| | WITH ARC | 82.78 | 85.02 | 83.65 |

**TABLE 3** Variation of open-circuit voltage of cells with mesa of 12.25 mm$^2$, 1 mm$^2$ and 0.076 mm$^2$ depending on the presence of an ARC

| Variation of open-circuit voltage (AM1.5D, 0.1 W·cm$^{-2}$, 25°C) | | Mesa area | | |
|---|---|---|---|---|
| | | 12.25 mm$^2$ | 1 mm$^2$ | 0.076 mm$^2$ |
| Comparison to the 12.25 mm$^2$-mesa reference cell | NO ARC | N/A | −6.75% | −13.16% |
| | WITH ARC | N/A | −5.81% | −10.79% |
| ARC effect | | +2.30% | +3.33% | +5.10% |

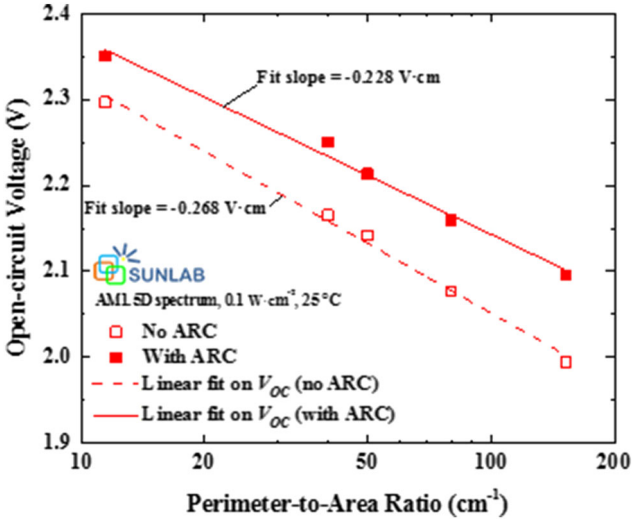


**FIGURE 6** Open-circuit voltage as a function of perimeter-to-area ratio (mesa) of fabricated rectangular cells without and with ARC (one cell per size) [Colour figure can be viewed at wileyonlinelibrary.com]

Assuming the one-diode model for each subcell and neglecting the resistances and the tunnel junction effects, one can express the open-circuit voltage of a three-junction solar cell under one sun as follows:

$$V_{OC} \approx \sum_{i=1}^{3} \frac{n^i kT}{q} \ln\left[\frac{J_L^i}{J_0^i}\right] \quad (1)$$

where $n^i$ is the diode ideality factor of subcell $i$ in the multijunction cell, $k$ is the Boltzmann constant, $T$ is absolute temperature, $q$ is the electron charge, $J_L^i$ is the photogenerated current density of subcell $i$, and $J_0^i$ is the saturation current density of subcell $i$. The quasi-linear decrease of $V_{OC}$ vs $\log_{10}(P_{mesa}/A_{mesa})$ indicates that $J_0^i$ varies inversely proportional with the $P_{mesa}/A_{mesa}$ and is therefore strongly dominated by recombination current at the junction perimeter. Indeed, based on a two-diodes model for the subcells, the saturation current density in a subcell is

$$J_0^i = J_{01}^i + J_{02,SRH}^i + J_{02,per}^i \quad (2)$$

where $J_{01}^i$ is the saturation current of subcell $i$ associated to drift/diffusion (ideality factor of 1), $J_{02,SRH}^i$ is the saturation current density of subcell $i$ due to Shockley-Read-Hall recombinations (ideality factor of 2) and $J_{02,per}^i$ is the is the saturation current density of subcell $i$ due to surface recombination (ideality factor of 2) at the perimeter of the cell and can be expressed as follows:

$$J_{02,per}^i = 2qS_0^i L_S^i \frac{P_{mesa}}{A_{mesa}} \quad (3)$$

where $S_0^i$ is the surface recombination velocity at the perimeter and $L_S^i$ is the diffusion length. The decrease of the slope observed for the cells with passivating ARC indicates a reduction of the dark current of (at least) one cell with high recombination current at the junction perimeter, and therefore a decrease of the surface recombination velocity for this cell. Nonetheless, the linear variation even with passivating ARC indicates that perimeter recombination remains the dominating factor for (at least) one subcell even with passivating ARC. Indeed, $J_{01}^i$ and $J_{02,SRH}^i$ are inherent to the bulk recombinations and do not depend on perimeter effect. An optimized passivating ARC would however lower the perimeter recombination rate.

## 3.2 | Measurements under concentration

Two rectangular cells having mesa areas of 0.25 mm$^2$ and 1 mm$^2$, both with ARC and 120 μm grid pitch, were electrically characterized under concentrated illumination at Fraunhofer Institute for Solar Energy Systems (ISE) in Freiburg, Germany. Despite our efforts, the full characterization under concentration of the 0.068 μm$^2$-mesa cells at either LN2, SUNLAB or ISE was not possible, mostly because of the predominant contribution of light reflection from the measurement probes and/or difficulty to get uniform spectral matching at the sub-millimeter scale.

The *I-V* curves measured under concentrated sunlight for the 1 mm$^2$ and 0.25 mm$^2$ cells are presented in Figure 7. For concentration factors above 450 suns for the 1-mm$^2$ cell and 584 suns for the 0.25-mm$^2$ cell, a kink around 2.7 V was measured, significantly decreasing the *FF*. This kink is representative of a current-density limitation by a tunnel junction within this epitaxial structure, similar to the behavior shown in Brunco et al.[39,40]

Figure 7 illustrates the open-circuit voltage, fill factor, and efficiency of a 0.25-mm$^2$ cell and a 1-mm$^2$ cell as a function of light concentration. The $\Delta V_{OC}$ observed due to size difference, and so perimeter recombination effect, is 3.8% under one sun and falls down to 1.1% under ~970 suns (obtained by interpolation). This effect is attributed to a saturation effect of perimeter states that makes recombination less significant under high concentration.[24] Using flash

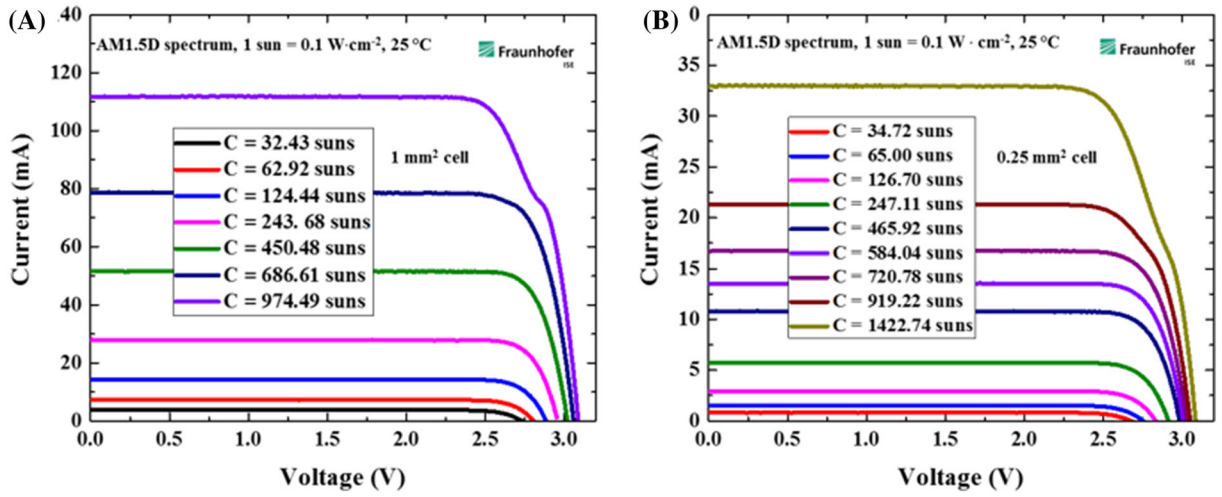


**FIGURE 7** Current–voltage characteristics of a (A) 1-mm$^2$ mesa cell and (B) a 0.25-mm$^2$ mesa rectangular cell under concentrated light [Colour figure can be viewed at wileyonlinelibrary.com]

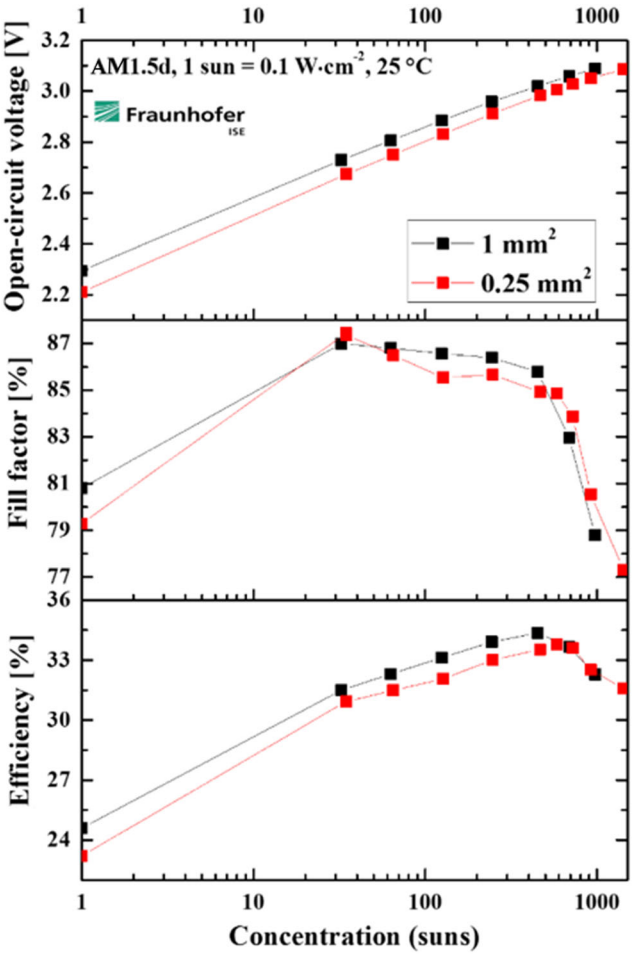


**FIGURE 8** Open-circuit voltage (top), fill factor (middle), and efficiency (bottom) of a 0.25-mm$^2$ and a 1-mm$^2$ (mesa area) solar cell under concentrated light [Colour figure can be viewed at wileyonlinelibrary.com]

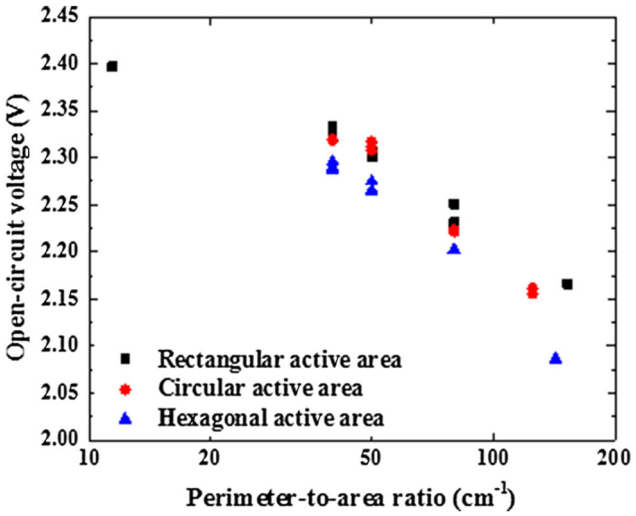


**FIGURE 9** Open-circuit voltage as a function of perimeter-to-area ratio (mesa) for different cell active area geometries [Colour figure can be viewed at wileyonlinelibrary.com]

tests in open-circuit conditions at LN2, similar trends were observed for cells with mesa area ranging from 12.25 to 0.076 mm$^2$ (see Appendix B).

Multiple effects seem to affect the *FF* including the tunnel junction limitations discussed above. It can be first seen that in both cells the *FF* peaks at a very low concentration (highest *FF* = 87.4% under 35 suns for the 0.25-mm$^2$ cell and *FF* = 87.0% under 32 suns for the 1-mm$^2$ cell) and decreases slowly when the concentration increases. When high concentration is reached (721 suns for 0.25 mm$^2$ cell and 687 suns for 1 mm$^2$ cell), the *FF* drops very rapidly when concentration is further increased and kinks start to be visible on the *I-V* curves. The *FF* of the smaller cell is lower than the one of the 1-mm$^2$ cell for

**TABLE 4** Variation of open-circuit voltage of a 12.25-mm$^2$ cell and a 0.076-mm$^2$ cell (mesa area, rectangular cells) depending on the light intensity (under 1 sun and approximately 1330 suns)

| Variation of open-circuit voltage (*AM1.5D, 1 sun = 0.1 W·cm$^{-2}$, 25°C*) | Mesa area | | |
|---|---|---|---|
| | 12.25 mm$^2$ | 0.076 mm$^2$ | Difference due to mesa area |
| 1 sun | 2.350 | 2.096 | −10.8% |
| ~1330 suns | 3.145 | 3.028 | −3.7% |
| Difference due to light intensity | +33.8% | +44.5% | N/A |

concentration below 584 sun (except under 35 suns) and is larger afterward.

Finally, due to these *FF* variations, a maximum efficiency of 34.4% is reached under 450 suns by the 1-mm$^2$ cell and 33.8% under 584 suns by the 0.25-mm$^2$ cell (normalized by active area, i.e. mesa area to which busbars area was excluded). Lower current and lower series resistance in smaller cells are expected to shift the maximum efficiency to higher concentration. This effect is observed in our data but is partly hidden by the predominance of the tunnel junction limitation under high concentration. It is however expected that both cells could reach the highest efficiency under very high concentration (>1000 suns) with adjusted tunnel junctions.

## 4 | CONCLUSION

Micro-modules are gaining interest over recent years as they promise to exploit the high efficiency of microcells at a reduced LCOE. However, some hurdles remain on the way to their wide deployment. We demonstrated InGaP/InGaAs/Ge solar cells with various shapes and total surface down to 0.089 mm$^2$, fully fabricated with a dedicated microfabrication process that used plasma etching for isolation and singulation steps. The improved wafer area utilization offered by plasma dicing removes one of the major barriers of the development of microcells. The fabricated cells have shown good electrical performance with $V_{OC}$ = 2.350 V and *FF* = 82.7% for the 12.25-mm$^2$-mesa reference cell under one-sun illumination. However, a degradation of the electrical performance was observed when reducing cell areas with up to 10.2% drop in $V_{OC}$ for cells without ARC. This tendency confirmed the inherent impact of surface recombination at the perimeter of the cells. It was shown that the ARC can act as a passivation film, diminishing the perimeter recombination impact on very small cells under one sun illumination. Flash measurements have also shown that limitation of the perimeter recombination impact is observed under high intensity light. Finally, microcells have demonstrated good electrical performance (33.8% under 584 suns for the 0.25 mm$^2$ cell), which limitation under very high concentration was attributed to a tunnel junction issue rather than resistive losses. Adjusted tunnel junctions may therefore lead to a higher efficiency to be reached by the microcells under very high concentration, opening the path for their wide use in micro-CPV.

## ACKNOWLEDGEMENTS

LN2 is a joint International Research Laboratory (Unité Mixte de Recherche IRL 3463) funded and co-operated by Université de Sherbrooke (Canada) and CNRS (France) as well as INSA Lyon, ECL, Université Grenoble Alpes (UGA) as well as the French national nanofabrication network RENATECH. The authors acknowledge FRQNT, PROMPT and CNRS for financial support. We acknowledge funding support from the Natural Sciences and Engineering Research Council of Canada, NSERC CREATE TOP-SET no.497981 and MARS-CPV.

## ORCID

*Pierre Albert* https://orcid.org/0000-0003-3383-4960
*Abdelatif Jaouad* https://orcid.org/0000-0002-1466-7346
*Christopher E. Valdivia* https://orcid.org/0000-0002-6072-2959
*Yannick Deshayes* https://orcid.org/0000-0002-1328-1724
*Karin Hinzer* https://orcid.org/0000-0002-2414-6288
*Laurent Béchou* https://orcid.org/0000-0002-0920-3619
*Vincent Aimez* https://orcid.org/0000-0002-1594-3242
*Maxime Darnon* https://orcid.org/0000-0002-6188-7157

## REFERENCES

1. Green MA, Hishikawa Y, Dunlop ED, et al. Solar cell efficiency tables (Version 53). *Prog Photovolt Res Appl*. 2019;27(1):3-12. https://doi.org/10.1002/pip.3102
2. Scott M. Clean energy will continue to hit dirty power as costs continue to fall. *Forbes*. 2019. https://www.forbes.com/sites/mikescott/2019/10/29/clean-energy-will-continue-to-hit-dirty-power-as-costs-continue-to-fall/
3. Philipps SP, Bett AW, Horowitz K, Kurtz S. Current status of concentrator photovoltaic (CPV) technology 2017. https://doi.org/10.2172/1351597
4. Algora C, Rey-Stolle I, Galiana B, et al. III-V concentrator solar cells as LEDs. *III-Vs Rev*. 2005;18(6):40-42. https://doi.org/10.1016/S0961-1290(05)71233-3
5. Sandwell P, Duggan G, Nelson J, Ekins-Daukes N. The environmental impact of lightweight HCPV modules: efficient design and effective deployment. *Prog Photovolt Res Appl*. 2016;24(11):1458-1472. https://doi.org/10.1002/pip.2802
6. Domínguez C, Jost N, Askins S, Victoria M, Antón I. A review of the promises and challenges of micro-concentrator photovoltaics, 2017 13th International Conference on Concentrator Photovoltaic Systems (CPV), 080003. https://doi.org/10.1063/1.5001441
7. Yamada N, Ijiro T, Goto W, Okamoto K, Dobashi K, Shiobara T. Development of silicone-encapsulated CPV module based on LED package technology. *Spec Conf (PVSC)*. 2013 IEEE 39th Photovolt;493-496. https://doi.org/10.1109/PVSC.2013.6744197

8. Nishioka K, Takamoto T, Agui T, Kaneiwa M, Uraoka Y, Fuyuki T. Evaluation of InGaP/InGaAs/Ge triple-junction solar cell and optimization of solar cell's structure focusing on series resistance for high-efficiency concentrator photovoltaic systems. *Sol Energy Mater sol Cells*. 2006;90(9):1308-1321. https://doi.org/10.1016/j.solmat.2005.08.003
9. Vossier A, Hirsch B, Katz EA, Gordon JM. On the ultra-miniaturization of concentrator solar cells. *Sol Energy Mater sol Cells*. 2011;95(4):1188-1192. https://doi.org/10.1016/j.solmat.2010.12.053
10. Ritou A, Voarino P, Raccurt O. Does micro-scaling of CPV modules improve efficiency? A cell-to-module performance analysis. *Sol Energy*. 2018;173:789-803. https://doi.org/10.1016/j.solener.2018.07.074
11. Itou A, Asano T, Inoue D, et al. High-efficiency thin and compact concentrator photovoltaics using micro-solar cells with via-holes sandwiched between thin lens-array and circuit board. *Jpn J Appl Phys*. 2014;53:04ER01-1–04ER01-5. https://doi.org/10.7567/JJAP.53.04ER01
12. Fidaner O, Suarez FA, Wiemer M, et al. High efficiency micro solar cells integrated with lens array. *Appl Phys Lett*. 2014;104(10):103902-1–103902-5. https://doi.org/10.1063/1.4868116
13. Sheng X, Bower CA, Bonafede S, et al. Printing-based assembly of quadruple-junction four-terminal microscale solar cells and their use in high-efficiency modules. *Nat Mater*. 2014;13(6):593-598. https://doi.org/10.1038/nmat3946
14. Ghosal K, Fisher B, Lilly D, Gabriel J, Seel S, Burroughs S. Ultrahigh Efficiency HCPV Modules and systems. *IEEE J Photovolt*. 2016;6(5):1360-1365. https://doi.org/10.1109/JPHOTOV.2016.2590884
15. Hayashi N, Inoue D, Matsumoto M, et al. High-efficiency thin and compact concentrator photovoltaics with micro-solar cells directly attached to a lens array. *Opt Express*. 2015;23(11):A594-A603. https://doi.org/10.1364/OE.23.00A594
16. Ritou A, Voarino P, Goubault B, David N, Bernardis S, Raccurt O, et al. Mechanical tolerances study through simulations and experimental characterization for a 1000X micro-concentrator CPV module, 2017 13th International Conference on Concentrator Photovoltaic Systems (CPV), 030007. https://doi.org/10.1063/1.5001418
17. Chinello E, Modestino MA, Coulot L, et al. A 25.1% Efficient standalone solar Chloralkali generator employing a microtracking solar concentrator. *Glob Chall*. 2017;1(9):1700095-1–1700095-8. https://doi.org/10.1002/gch2.201700095
18. Lumb MP, Mack S, Schmieder KJ, et al. GaSb-based solar cells for full solar spectrum energy harvesting. *Adv Energy Mater*. 2017;7(20):1700345-1–1700345-9. https://doi.org/10.1002/aenm.201700345
19. Chang GS, Hwang WC, Wang YC, Yang ZP, Hwang JS. Determination of surface state density for GaAs and InAlAs by room temperature photoreflectance. *J Appl Phys*. 1999;86(3):1765-1767. https://doi.org/10.1063/1.370961
20. Stellwag TB, Dodd PE, Carpenter MS, Lundstrom MS, Pierret RF, Melloch MR, et al. Effects of perimeter recombination on GaAs-based solar cells, 1990 IEEE 21st Photovolt. Spec. Conf. (PVSC), 442–447. https://doi.org/10.1109/PVSC.1990.111663
21. Belghachi A, Khelifi S. Modelling of the perimeter recombination effect in GaAs-based micro-solar cell. *Sol Energy Mater sol Cells*. 2006;90(1):1-14. https://doi.org/10.1016/j.solmat.2005.01.009
22. Gu T, El-Emawy MA, Yang K, Atintz A, Lester LF. Suppression of edge recombination in InAs/InGaAs DWELL solar cells. *MRS Proc*. 2009;1210:1210-Q02-07. https://doi.org/10.1557/PROC-1210-Q02-07
23. Espinet-González P, Rey-Stolle I, Ochoa M, Algora C, García I, Barrigón E. Analysis of perimeter recombination in the subcells of GaInP/GaAs/Ge triple-junction solar cells: analysis of perimeter recombination. *Prog Photovolt Res Appl*. 2015;23(7):874-882. https://doi.org/10.1002/pip.2501
24. Wiesenfarth M, Steiner M, Helmers H, Bett AW. Voltage losses due to the perimeter and dark area in micro-concentrator solar cells. *Sol Energy Mater sol Cells*. 2021;219:110791-1–110791-10. https://doi.org/10.1016/j.solmat.2020.110791
25. Zhou L, Bo B, Yan X, Wang C, Chi Y, Yang X. Brief review of surface passivation on III-V semiconductor. *Crystals*. 2018;8(5):226-1–226-14. https://doi.org/10.3390/cryst8050226
26. Huo P, Rey-Stolle I. Al-based front contacts for HCPV solar cell. In: *2017 13th International Conference on Concentrator Photovoltaic Systems (CPV)* 040004. https://doi.org/10.1063/1.5001426
27. Albert P, Jaouad A, Darnon M, Valdivia C E, Volatier M, Deshayes Y, et al. Front-contacted multijunction micro cells: fabrication and characterization. Presented in 2018 14th International Conference on Concentrator Photovoltaic Systems (CPV).
28. Homier R, Jaouad A, Turala A, et al. Antireflection coating design for triple-junction III–V/Ge high-efficiency solar cells using low absorption PECVD silicon nitride. *IEEE J Photovolt*. 2012;2(3):393-397. https://doi.org/10.1109/JPHOTOV.2012.2198793
29. Dicing products hub blades and services for advanced material applications. Kulicke & Soffa Company. https://www.seas.upenn.edu/~nanosop/documents/dicing_blade_catalog.pdf
30. Martin D, Sullivan S. Dicing of MEMS devices. *Handb. Silicon-Based MEMS Mater. Technol. Elsevier*. 2010;671-677.
31. Van Borkulo J, Evertsen R, Hendriks R. Enabling technology. In: *Thin Wafer Dicing*. Shanghai, China: ECS: ECS Trans.; 2009:837-842 https://doi.org/10.1149/1.3096543
32. Darnon M, de Lafontaine M, Volatier M, et al. Deep germanium etching using time multiplexed plasma etching. *J Vac Sci Technol B Nanotechnol Microelectron Mater Process Meas Phenom*. 2015;(6):060605-1–060605-7. https://doi.org/10.1116/1.4936112
33. de Lafontaine M, Pargon E, Gay G, et al. Anisotropic and low damage III-V/Ge heterostructure etching for multijunction solar cell fabrication with passivated sidewalls. *Micro and Nano Engineering*. 2021. https://doi.org/10.1016/j.mne.2021.100083
34. de Lafontaine M, Pargon E, Petit-Etienne C, et al. Influence of plasma process on III-V/Ge multijunction solar cell via etching. *Sol Energy Mater sol Cells*. 2019;195:49-54. https://doi.org/10.1016/j.solmat.2019.01.048
35. de Lafontaine M, Darnon M, Jaouad A, et al. Plasma etching applications in concentrated photovoltaic cell fabrication. In: *12th International Conference on Concentrator Photovoltaic Systems (CPV)*; 2016 p. 060001. https://doi.org/10.1063/1.4962091
36. de Lafontaine M, Darnon M, Colin C, et al. Impact of via hole integration on multijunction solar cells for through cell via contacts and associated passivation treatment. *IEEE J Photovolt*. 2017;7(5):1456-1461. https://doi.org/10.1109/JPHOTOV.2017.2711423
37. Adachi S. Chemical etching of InGaAsP/InP DH wafer. *J Electrochem Soc*. 1982;129(5):1053-1062. https://doi.org/10.1149/1.2124014
38. Savriama G. Review of laser technologies for dicing microelectronics chips. 2016:169–178. https://doi.org/10.13140/RG.2.1.1159.9129
39. Brunco DP, Jaeger B, Eneman G, et al. Germanium MOSFET devices: advances in materials understanding. *Process Development, and Electrical Performance*. 2008;155(7):552-561. https://doi.org/10.1149/1.2919115
40. Andreev VM, Ionova EA, Larionov VR, Rumyantsev VD, Shvarts MZ, Glenn G. Tunnel diode revealing peculiarities at I-V measurements in multijunction III-V solar cells. In: *IEEE 4th World Conf. Photovolt. Energy Conf*. Vol. 2006. IEEE; 2006:799-802. https://doi.org/10.1109/WCPEC.2006.279577

**How to cite this article:** Albert P, Jaouad A, Hamon G, et al. Miniaturization of InGaP/InGaAs/Ge solar cells for micro-concentrator photovoltaics. *Prog Photovolt Res Appl*. 2021; 1–10. https://doi.org/10.1002/pip.3421

## APPENDIX A: $V_{OC}$ versus $P_{mesa}/A_{mesa}$ of cells with various geometries

In Figure 9 can be seen the open-circuit voltage of various geometries and dimensions cells, plotted against the perimeter-to-area ratio of mesas. Cells were made from the same sample. As observed in Figure 6, a quasi-linear decrease of $V_{OC}$ vs. $P_{mesa}/A_{mesa}$ can be observed for each geometries. The various points for a given geometry and a given $P_{mesa}/A_{mesa}$ stand for the various contact designs while the mesa area is similar. The differences in $V_{OC}$ observed for a given $P_{mesa}/A_{mesa}$ can therefore be attributed to large dark current density due to the shading induced by the top contacts. For example, considering the $P_{mesa}/A_{mesa}$ = 80 $cm^{-1}$, the shading in rectangular active area cells is comprised between 33.8% and 34.5%, while the one of circular active area cells is comprised between 48.2% and 49.0% and the shading in the hexagonal active area cell is 53.0%. Whereas this shading was identified as one the major limitation in Wiesenfarth et al,[24] it can be seen in Figure 9 that the voltage losses due to perimeter effects is larger. For the given $P_{mesa}/A_{mesa}$ of 80 $cm^{-1}$, an average reduction of 0.99% and 1.90% in $V_{OC}$ is measured when the metal coverage proportion increases by 22.0% (circular active area) and 28.7% (hexagonal active area), respectively.

## APPENDIX B: Effect of light intensity on $V_{OC}$ depending on cell area

In Table 4 is shown the variation of the open-circuit voltage of rectangular cells with a 12.25-$mm^2$ mesa area and a 0.076-$mm^2$ mesa area. Both cells have an ARC and were made from the same sample. As discussed in section 3.2, high-intensity measurements of microcells are not straightforward. However, experiments have shown that measurements at open-circuit conditions ($V_{OC}$) tend to be more reliable whereas fluctuations cannot be excluded. For this reason, the light intensity presented is given to be approximately 1330 suns. In Table 4, it can be seen that the variation in $V_{OC}$ due to area decrease falls from 10.8% under one sun to 3.7% under approximately 1,330 suns. This proves the limitation of the effects of perimeter recombination under high-intensity light, predominant under one sun illumination in microcells. This behavior is confirmed by observing the gain when increasing the light intensity, which benefits more to the 0.076-$mm^2$ cell (with an increase of $V_{OC}$ of 44.5%) compared to the 12.25-$mm^2$ cell (with an increase of $V_{OC}$ of 33.8%).